Ultra-Low Doses of Chirality Sorted (6,5) Carbon Nanotubes for Simultaneous Tumor Imaging and Photothermal Therapy

Alexander L. Antaris,[†,⊥] Joshua T. Robinson,[‡,⊥] Omar K. Yaghi,[‡,⊥] Guosong Hong,[‡] Shuo Diao,[‡] Richard Luong,[§] and Hongjie Dai[‡,*]

[†]Department of Material Science and Engineering, Stanford University, Stanford, California 94305, United States, [‡]Department of Chemistry, Stanford University, Stanford, California 94305, United States, and [§]Department of Comparative Medicine, Stanford University School of Medicine, Stanford, California 94305, United States. [⊥]A.L.A., J.T.R, and O.M.Y. were equal contributors.

ABSTRACT

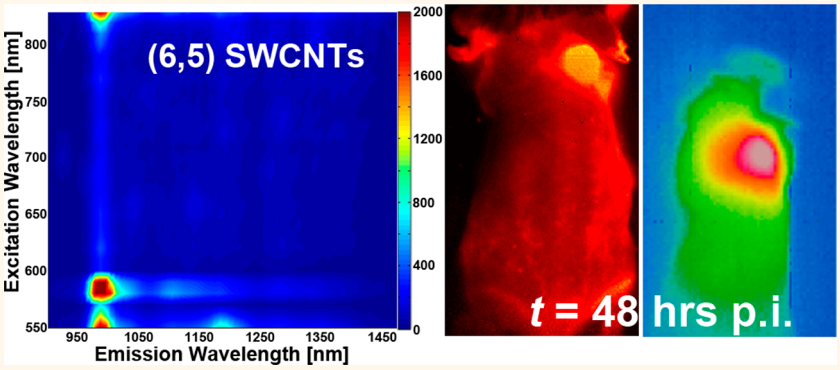

Single-walled carbon nanotubes (SWCNTs) exhibit intrinsic fluorescence and strong optical absorption in the near-infrared (NIR) biological window (0.7−1.4 μm), rendering them ideal for *in vivo* imaging and photothermal therapy. Advances in SWCNT sorting have led to improved nanoelectronics and are promising for nanomedicine. To date, SWCNTs used *in vivo* consist of heterogeneous mixtures of nanotubes and only a small subset of chirality nanotubes fluoresces or heats under a NIR laser. Here, we demonstrate that separated (6,5) SWCNTs exchanged into a biocompatible surfactant, C_{18}-PMH-mPEG, are more than 6-fold brighter in photoluminescence on the per mass basis, afford clear tumor imaging, and reach requisite photothermal tumor ablation temperatures with a >10-fold lower injected dose than as-synthesized SWCNT mixtures while exhibiting relatively low (6,5) accumulation in the reticuloendothelial system. The intravenous injection of ~4 μg of (6,5) SWCNTs per mouse (0.254 mg/kg) for dual imaging/photothermal therapy is, by far, the lowest reported dose for nanoparticle-based *in vivo* therapeutics.

KEYWORDS: single-walled carbon nanotubes · nanoelectronics · photothermal therapy

The unique properties of single-walled carbon nanotubes (SWCNTs) make them promising theranostic agents capable of tumor imaging while simultaneously providing treatment.[1−7] The intrinsic photoluminescence of SWCNTs renders them as nonphotobleaching fluorophores capable of high-resolution *in vivo* imaging and deep tissue penetration with excitation in the near-infrared-I (NIR-I, 700−900 nm) and emission in the near-infrared-II (NIR-II, 950−1400 nm) regions which fall within the biological transparency window (0.7−1.4 μm).[8−10] SWCNTs are capable of tumor accumulation through the enhanced permeability and retention (EPR) effect, a physical state describing tortuous tumor vasculature which increases tumor uptake of intravenously injected nanomaterials compared to healthy tissue.[1,11−13] Additionally, high light absorption of SWCNTs in the NIR affords tumor photothermal therapy at much lower laser powers than those needed for plasmonic nanomaterials.[2,14]

* Address correspondence to hdai1@stanford.edu.

Received for review February 6, 2013 and accepted March 22, 2013.

Published online March 23, 2013
10.1021/nn4006472

However, all biological studies to date incorporate as-synthesized SWCNTs containing many chiralities, the vast majority of which are off-resonance, lacking a unique absorption and emission peak, and thus extraneous when using a single excitation wavelength. Isolated SWCNT chiralities without off-resonance nanotubes would greatly reduce therapeutic doses, achieving imaging and treatment results at much lower doses than as-synthesized SWCNTs while alleviating toxicity concerns.[15,16]

Advancements in carbon nanotube sorting have translated into an increase in the performance of electronic devices ranging from photovoltaics to printed circuitry, and are beginning to be utilized for biomedical SWCNT applications.[17−20] Recently, gel filtration separated SWCNTs highly enriched in the (12,1) and (11,3) chiralities have been used for vessel imaging at a low injected dose for highly effective resonance excitation of these chiralities at 808 nm.[21] Therapeutic applications of chirality separated SWNTs have not been demonstrated thus far. Progress on carbon nanotube synthesis has yielded some control over generating SWCNTs with desirable properties, yet applications requiring monodispersed populations rely on post-synthetic separation strategies.[22−32] Innovative approaches to carbon nanotube chirality sorting include DNA sequence motifs that recognize a specific chirality, gel filtration methods,[27,33] and density gradient ultracentrifugation (DGU).[29] Recently introduced nonlinear density gradients are capable of isolating >10 different (*n*,*m*) species, while iterative DGU purification steps attained single chirality purities in excess of 98%.[16,34] However, DGU, as well as most other separation methods, almost exclusively produce SWCNTs coated in nonbiocompatible surfactants, preventing chirality sorted SWCNTs for biological applications thus far.[27,28,35,36]

Herein, combining a nonlinear DGU architecture with a second iterative DGU step, we extracted the (6,5) chirality from HiPCO-grown SWCNTs at a purity of ∼80%. We exchanged (6,5) SWCNTs into a 90 kDa C_{18}-PMH-mPEG surfactant[32,33] to obtain highly biocompatible (6,5) tubes with ultra-long blood circulation time and high tumor uptake after intravenous tail-vein injection, while preserving the (6,5) SWCNT's near-infrared photoluminescence (NIR PL) properties.[37,4] Using an ultra-low dose of intravenously injected (6,5) SWCNTs (∼4 μg per mouse) and a 980 nm laser to precisely match the E_{11} resonance peak of (6,5) SWCNTs at ∼991 nm, we were able to photothermally heat tumors in mice to over 50 °C while performing whole-animal NIR-PL imaging to visualize tumor accumulation beginning 48 h prior to treatment. Photoluminescence of the exchanged (6,5) SWCNTs was more than 6-fold brighter than exchanged HiPCO SWCNTs at the same mass concentration. *In vivo* tumor imaging and photothermal ablation were accomplished at an unprecedented low dose of 0.254 mg SWCNT/kg body weight (∼4 μg per mouse), the lowest reported dose for combined imaging and tumor treatment with any class of nanomaterials.[2]

RESULTS

(6,5) Separation and Surfactant Exchange. As-synthesized HiPCO SWCNTs are a mixture of many chiralities with diameters in a range of 0.7−1.1 nm.[16] Preparation of these SWCNTs for DGU included a 1 h horn sonication in 2% sodium cholate (SC), a 30 min bath sonication, and a 2 h crash-out step at 22 000*g* on a table-top centrifuge to remove any poorly dispersed aggregates. The decanted SWCNTs were balanced to 1.13 g/mL using iodixanol and inserted into a nonlinear density gradient formed by carefully pipetting 6 layers of varying volumes at densities ranging from 1.16 to 1.09 g/mL into a centrifuge tube and tilting it ∼10° from horizontal for 1 h to allow for interlayer diffusion to smooth out the density steps between layers. The surfactant loading in the gradient was 0.7% SC and 0.175% sodium dodecyl sulfate (SDS), previously demonstrated as the ideal surfactant ratio for isolating (6,5) in this gradient structure.[34] Ultracentrifugation led to the separation of small, semiconducting SWCNTs with the (6,5) chirality migrating to a low buoyant density as seen in Figure 1a. High (6,5) purities (88%) are attainable with a single ultracentrifugation step in a nonlinear density gradient, yet unfortunately the increase in SWCNT concentration required to produce enough (6,5) for *in vivo* use caused a drop in purity as evidenced by the first order metallic SWCNT excitations visible from 450 to 550 nm and the (9,1) peak at 921 nm (see Figure 1b).

A further iterative DGU step was performed by inserting the material from the first separation at the bottom of a second, linear density gradient with a SC:SDS ratio of 4:1 and an overall surfactant loading of 1% (see Supporting Information Table S1 for all separation details). This second iteration, known to concentrate semiconducting SWCNTs at low buoyant densities, ultimately boosted the (6,5) purity to ∼80% as seen by the suppressed metallic peak at 466 nm and the decreased (9,1) contamination while leaving a yellow band slightly enriched in metallic SWCNTs at a higher buoyant density (Figure 1d).[16] The photoluminescence (PLE) spectra (Figure 1e) of the twice-separated (6,5) fractions confirmed the absence of significant contamination from other chiralities.

The bile salt sodium cholate can solubilize SWCNTs in water; however, cholate dispersed SWCNTs aggregate when excess sodium cholate is removed from the solution.[38] This process occurs rapidly *in vivo*, making cholate-SWCNTs unusable for *in vivo* purposes. Similarly, SWCNTs coated in SDS are toxic because of the intrinsic toxicity of SDS in addition to lacking stability after excess SDS removal.[35] We employed a

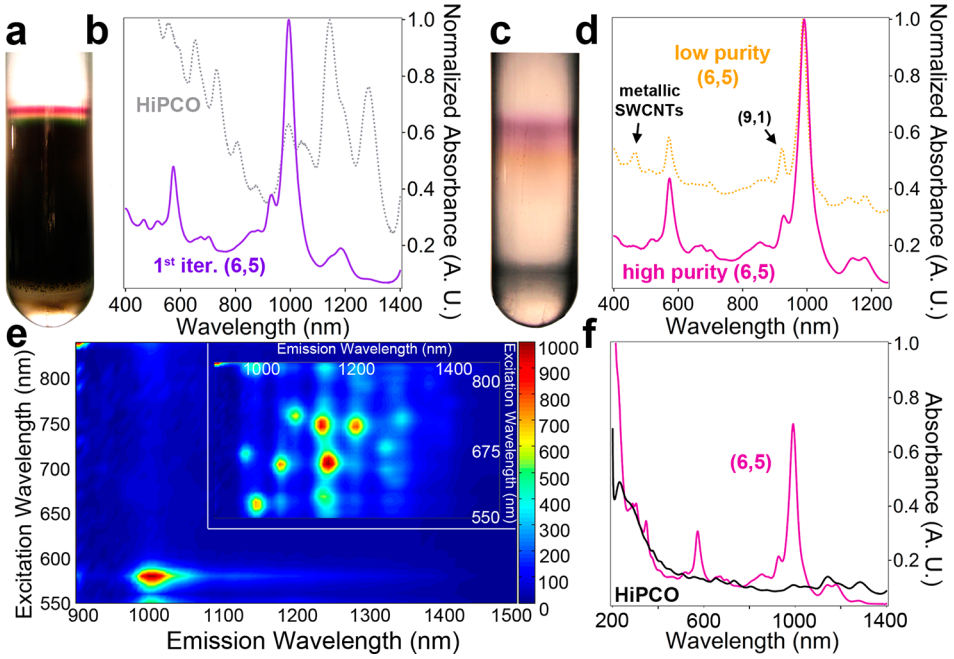

Figure 1. Isolation of (6,5) SWCNTs employing density gradient ultracentrifugation (DGU). (a and c) Photographs of centrifuge tubes following DGU after the first iteration in a nonlinear density gradient (a) and after the second iteration in a linear gradient (c). (b and d) Normalized absorbance spectra comparing (b) first iteration (6,5) to bulk HiPCO and the (d) pink (6,5) band to the yellow band at a higher buoyant density slightly enriched in metallic SWCNTs. (e) Photoluminescence spectra of (6,5) compared to as-synthesized HiPCO. (f) The absorbance spectra (1 mm path length) of the mass balanced (6,5) and HiPCO preceding intravenous injection.

surfactant-exchange method to replace SC and SDS coatings, as well as any residual iodixanol, with C_{18}-PMH-mPEG, a biocompatible, PEGylated surfactant with excellent pharmacokinetics when coating SWCNTs.[39] With the use of a 12−14 kDa MWCO dialysis membrane, SC and SDS were selectively removed from the surface of the separated SWCNTs during 8 water bath exchanges while the much larger 90 kDa C_{18}-PMH-mPEG remained trapped in the membrane. An initial 5 min bath sonication after adding C_{18}-PMH-mPEG to the (6,5) SWCNTs combined with a very short (∼2 min) bath sonication between each water change facilitated the adsorption of C_{18}-PMH-mPEG onto the carbon nanotube surface. During centrifugation and washing, a reasonable (∼50%) physical yield of still soluble, individualized (6,5) SWCNTs was obtained with an acceptable (∼60%) loss of NIR PL quantum yield (see Supporting Information Figure S4).[4] After dialysis, excess C_{18}-PMH-mPEG was removed during multiple wash steps through a centrifuge tube filter. The average length of the exchanged (6,5) SWCNTs was ∼228 nm (see Supporting Information Figure S5), much longer than carbon nanotubes directly sonicated in C_{18}-PMH-mPEG (140 nm).[2]

NIR Laser Heating of (6,5) SWCNTs in Solutions. Extraction of high purity (6,5) SWCNTs increased absorption on a per mass basis compared to a random mixture of carbon nanotubes as the 980 nm laser used for heating is in near-resonance with the (6,5) E_{11} peak. After exchanging the (6,5) and bulk HiPCO SWCNTs into C_{18}-PMH-mPEG, both nanotube suspensions were mass balanced by matching the optical absorbance at the $\pi-\pi^*$ interband transition peak of ∼4.5 eV and reading out the SWCNT content through HiPCO's published absorption coefficient of ∼46.5 L/g*cm at 808 nm.[6] As the $\pi-\pi^*$ interband transition directly correlates with the amount of graphitic material present, this method has previously demonstrated its ability to mass balance near-single chirality SWCNT populations.[40] Additionally, unlike the π-plasmon peak at higher energies, the $\pi-\pi^*$ interband transition is not affected by the choice of surfactant coating or by the dielectric strength of the solution.[41] The $\pi-\pi^*$ interband transition normalization method gave a (6,5) mass extinction coefficient of 316 L/g*cm at the E_{11} peak (991 nm), which was within the error range of published values of 366.6 ± 80.7 L/g*cm determined by fluorescence labeling and AFM imaging (see Supporting Information Figure S6).[42]

At a concentration of 3.2 μg/mL determined by the method above, 50 μL each of (6,5), HiPCO, and PBS was irradiated with a 980 nm laser for 3 min at 0.6 W/cm^2. After the first minute of irradiation, the (6,5) maintained a ∼10 °C higher temperature than HiPCO throughout the course of irradiation and ultimately reached 53.4 °C. After 3 min, the HiPCO SWCNTs only heated to 43.5 °C (see Figure 2), confirming that the much stronger (6,5) absorbance peak at 980 nm translated into large differences in the photosensitizers' heating performance.

***In Vivo* (6,5) SWCNT Tumor Imaging.** The relative photoluminescence of HiPCO, first iteration (6,5), and second iteration (6,5), all mass balanced and exchanged into C_{18}-PMH-mPEG, was determined by excitation at 808 nm at a power density of 0.14 W/cm^2 and collecting the resulting emission from 900 to 1400 nm on an InGaAs camera with an exposure of 100 ms. Compared to as-synthesized HiPCO, the brightness of the first iteration (6,5) increased by 4.5×, while the second iteration (6,5) was ultimately 6.3× brighter (Figure 3a). An ultra-low dose of ~4 μg of second iteration (6,5) and unseparated HiPCO SWCNTs was intravenously injected into two groups (n = 4) of xenograft murine 4T1 breast tumor-bearing balb/c mice at equivalent carbon nanotube dosages (0.254 mg/kg), corresponding to a 14-fold lower dose than previously used for SWCNT tumor imaging and photothermal therapy.[2] Over the course of 48 h, the mice were imaged, giving clear, crisp definition of the murine breast cancer model 4T1 tumors, suggesting high levels of accumulation of the 90 kDa C_{18}-PMH-mPEG coated (6,5) SWCNTs within the tumor. A representative mouse with a subcutaneous tumor located laterally on the right shoulder showed a high signal at the site of the tumor with little detectable signal in the surrounding healthy tissue at each imaging time point (Figure 3e–g). Unseparated HiPCO injected mice did not give clear images (Figure 3c), while those injected with PBS had no discernible signal (Figure 3b), indicating the near absence of autofluorescence in the NIR-II region.[4]

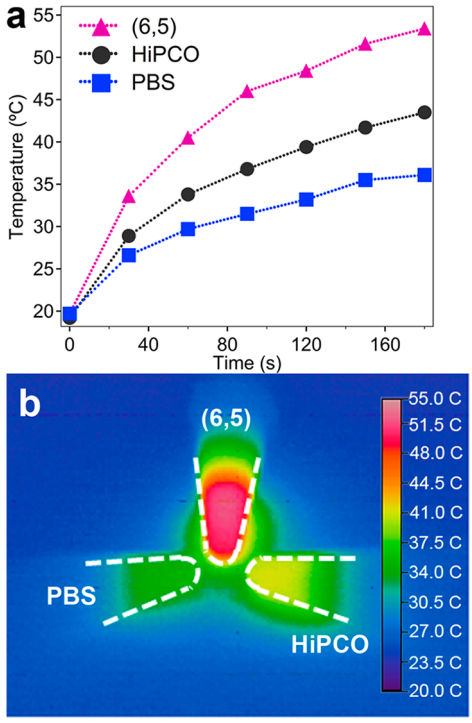

Figure 2. The (6,5) solution heating with irradiation in the NIR-II. (a) 50 μL of (6,5) and HiPCO SWCNTs at a concentration of 3.2 μg/mL and dispersed in 90 kDa C_{18}-PMH-mPEG, along with a PBS control, were heated for 3 min at 980 nm at a laser power density of 0.6 W/cm^2 and the average vial temperature was recorded every 30 s. (b) A thermal image of the (6,5), HiPCO, and PBS vial after 3 min of irradiation.

***In Vivo* (6,5) SWCNT Mediated Photothermal Tumor Ablation.** After 48 h of time course imaging, we investigated the theranostic capabilities of the separated (6,5) SWCNTs. Mice (n = 4) injected with the ultra-low dose (0.254 mg/kg) of SWCNTs underwent photothermal treatment by irradiation with a 980 nm laser at a power density of 0.6 W/cm^2 when the tumors were approximately ~46 mm^3 on average. Thermal images were

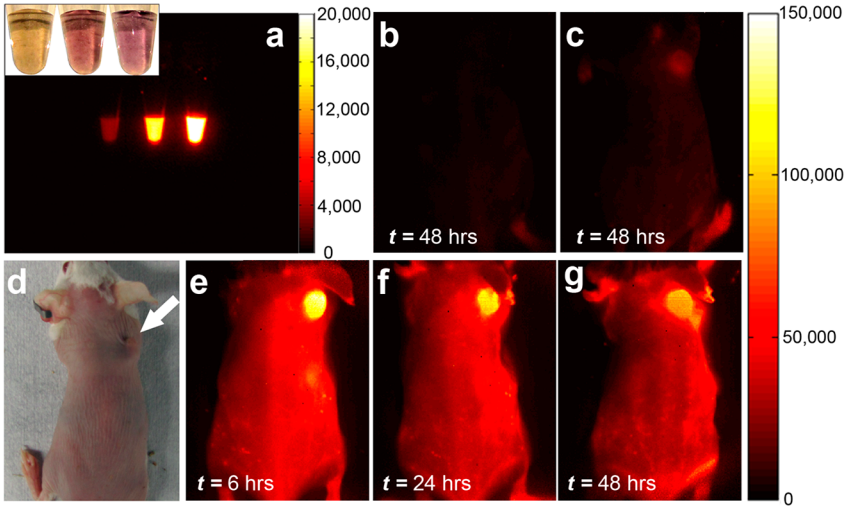

Figure 3. NIR (6,5) photoluminescence and time course fluorescence imaging in the NIR-II. (a) An optical and NIR PL image of 50 μL of C_{18}-PMH-mPEG dispersed as-synthesized HiPCO, first iteration (6,5), and second iteration (6,5), from left to right, at a concentration of 22.2 μg/mL. (b and c) NIR-II fluorescent images of a 4T1 tumor bearing mouse injected with (b) PBS and (c) HiPCO. (d) Optical image of a mouse bearing a 4T1 tumor on the right shoulder. (e–g) NIR-II fluorescent time course imaging 12, 24, and 48 h postinjection, from left to right, showing clear SWCNT accumulation in the 4T1 tumor. All mice were injected with 0.254 mg/kg of SWCNTs and emission collected from 0.9 to 1.4 μm after excitation at 808 nm at a laser power density of 0.14 W/cm^2. The scale bar on the right corresponds to all NIR images of 4T1 tumor bearing balb/c mice.

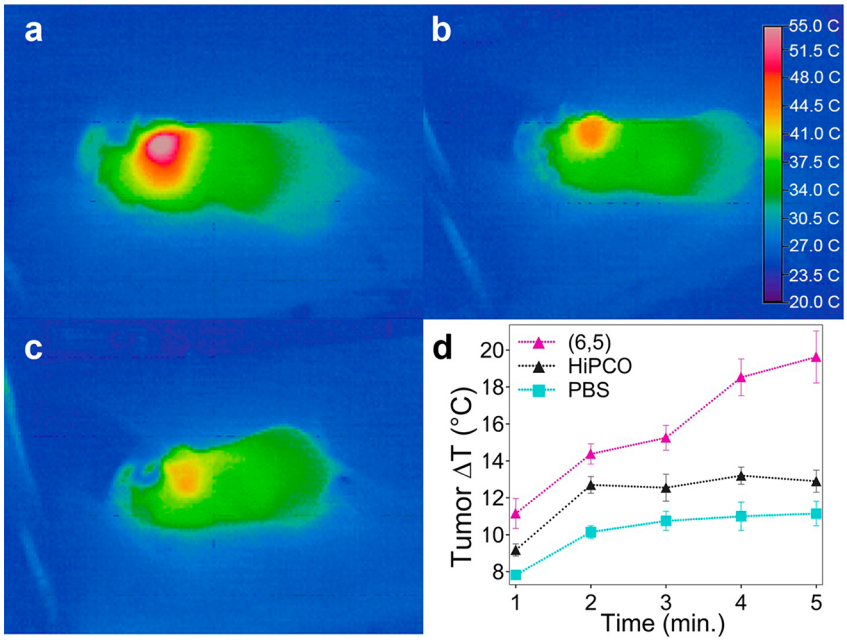

Figure 4. Photothermal ablation trial study in the NIR-II employing highly enriched (6,5) SWCNTs. (a−c) Representative thermal images from 4T1 tumor bearing balb/c mice ($n = 4$) 48 h after injection with 0.254 mg/kg of C_{18}-PMH-mPEG dispersed (a) (6,5) SWCNTs, (b) HiPCO SWCNTs, and (c) PBS control after 5 min of 980 nm laser irradiation at a power density of 0.6 W/cm^2. (d) The change in the average temperature of the 4T1 tumor mass as measured over the 5 min course of NIR-II laser treatment. The average starting body temperature was 33.0 °C.

taken before heating and at each minute during the 5 min of irradiation to measure the average tumor temperature over the course of treatment. A representative thermal image from each group, including the PBS control, is shown (Figure 4a−c) immediately before shutting off the laser. Mice in the (6,5) group experienced an average temperature increase of 19 °C during the course of treatment, reaching an average temperature of 51 °C after 5 min of irradiation (Figure 4d). On the basis of the Arrhenius damage integral and experimental studies, tumors in the (6,5) group reached requisite temperatures for successful tumor photoablation. Conversely, mice injected with HiPCO showed a 12 °C temperature increase during treatment and only heated approximately 2 °C more than the PBS control at each time point during the 5 min of irradiation. Mice injected with both HiPCO and PBS showed a rise in temperature yet failed to reach the photoablation limit of 50 °C (Figure 4d). All tumors treated with HiPCO SWCNTs continued to grow unabated. In the (6,5) group, 3 of the mice were successfully treated and showed no signs of regrowth during a post-treatment monitoring period of 1.5 months. This trial study clearly demonstrate the potential benefits of (6,5) SWCNTs over unsorted SWCNTs as promising photothermal and imaging agents.

(6,5) SWCNT Biodistribution and Blood Circulation Behavior. The biodistribution and circulation half-life of (6,5) was determined with a second group ($n = 3$) of balb/c mice bearing 4T1 tumors located laterally on both sides. Blood was collected periodically post intravenous injection and, using the intrinsic Raman `G' band of (6,5) SWCNTs, the % injected dose/gram blood (%ID/g) was determined (Figure 5b). Fitting a first-order exponential decay yielded an impressive blood circulation

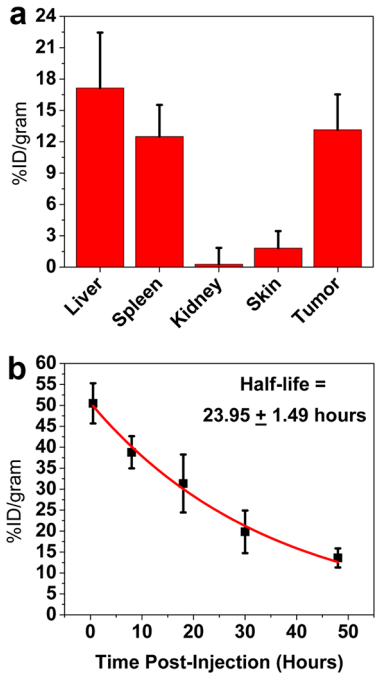

Figure 5. Biodistribution and circulation half-life of (6,5) SWCNTs exchanged into 90 kDa C_{18}-PMH-mPEG. (a) The biodistribution of 4T1 tumor bearing balb/c mice ($n = 3$) 72 h after injection with (6,5) SWCNTs (see Methods). (b) The concentration of (6,5) SWCNTs in blood ($n = 5$) over 48 h and fit with a first-order exponential decay model (red curve).

half-life of 23.95 ± 1.49 h, suggesting the ability of (6,5) SWCNTs to avoid uptake by the reticuloendothelial (RES) system. Three days post-injection, 3 mice were sacrificed for *ex vivo* organ analysis by Raman spectroscopy following previously published methods. The levels of (6,5) SWCNTs in the heart, lungs, pancreas, small intestine, and stomach were below the biodistribution detection limit.[43]

The average (6,5) SWCNT accumulation within the liver and the spleen of the RES system was low, ~17 and 12%ID/g respectively, nearly on the same level as the tumor uptake of the (6,5) tubes at ~13%ID/g (Figure 5a).[2,13] Three mice from the exchanged (6,5) SWCNT photothermal treatment group were sacrificed after confirming successful tumor ablation and submitted for histological staining 100 days after intravenous injection. Clinical blood chemistry and hematology panels showed completely normal analyte levels and no residual SWCNT bundles were found in any organ after a histological analysis (Supporting Information Figures S7 and S8). We observed no obvious toxicity in our trial studies (Supporting Information Figure S8). However, future work will be needed to fully address the long-term accumulation and toxicity of the single-chirality SWCNTs.

DISCUSSION

While very small quantities of SWCNTs are capable of producing a large number of electronic devices, the quantities needed for biomedical uses, particularly as a theranostic agent, are much higher. Separation methods, although still in infancy, are showing signs of promise for isolating sufficient amounts of near-single chirality SWCNT populations for *in vivo* use. We demonstrated that iterative DGU separations allowed for the collection of a sufficient quantity of (6,5) SWCNTs to treat tumors in mouse models using an unprecedented low dose. This is the first *in vivo* application of near single-chirality SWCNTs for effective tumor photoablation.

The selection of 808 nm for (6,5) excitation and imaging is not intuitive as (6,5) SWCNTs do not possess an absorption peak at this wavelength. The E_{22} transition of (6,5), where SWCNTs are typically excited, is located at 570 nm. However, recent studies have shown that (6,5) SWCNTs can be excited through a Raman-coupled mode at 808 nm with emission at 980 nm.[44] The 808 nm excitation is in near-resonance with an emission shoulder associated with (6,5) SWCNTs derived from a phonon-coupled transition. This process occurs when the SWCNT simultaneously absorbs a photon and creates a phonon, ultimately producing an emission identical to that of the (6,5) excitonic emission.[44] The high brightness of the (6,5) chirality is remarkable especially as the surfactant exchange process decreases fluorescence by up to 60% (see Supporting Information Figure S4). Excitation in the NIR-I region at 808 nm confers additional advantages such as better depth penetration and improved signal-to-noise ratios when imaging in the NIR-II with mouse models, especially compared to an excitation at (6,5)'s E_{22} at 570 nm which is limited in depth penetration due to high biological tissue and hemoglobin absorption.[8,45] Previous studies using bulk SWCNTs as *in vivo* fluorophores for organ identification, vessel imaging, and tumor imaging have all used an excitation wavelength of 808 nm in the NIR-I window for this reason.[4,8,13]

For the past decade, gold nanoparticles have been the standard for photothermal therapy. Gold-based photosensitizers require much higher injected doses to achieve tumor elimination with a reasonable laser power density. An intravenously injected (i.v.) dose of 50 mg/kg of gold nanocages [compared to the 0.254 mg/kg dose for (6,5) SWNTs] is necessary for *in vivo* tumor heating.[46] Gold nanorods required a dose of 20 mg/kg to completely eliminate tumors using 2 W/cm^2 NIR-I laser.[14] The absorption data of separated SWCNTs *versus* gold nanoparticles can explain the decreased dose. On a per mass basis, single-chirality SWCNTs in strong resonance with a laser will absorb 10−20× more light than optimized gold nanorods or nanoparticles.[2] Also, the atomic mass of carbon is only ~$^1/_{16}$ that of gold.

Biocompatible carbon-based nanomaterials, due to high NIR light absorption, have increasingly been used as photosensitizing agents for *in vivo* photothermal therapy. Graphene oxide, a slightly oxidized single-layered graphene sheet, was able to achieve efficient tumor elimination with injected doses of 20 mg/kg.[47] SWCNTs possess superior NIR absorption compared to graphene owing to their Van Hove singularities; intravenously injected unseparated SWCNTs were able to ablate tumors through photothermal therapy at doses as low as 3.6 mg/kg, the lowest dose reported until now of intravenously injected photosensitizers used for *in vivo* photothermal therapy.[2,48] Using (6,5) SWCNTs, we were able to achieve an even lower dose of 0.254 mg/kg for photothermal therapy than studies that directly injected SWCNTs and MWNTs into the tumor.[49,50] Nevertheless, even though the (6,5) SWCNTs are resonantly photothermally heated at 980 nm, we do note a pitfall of nonspecific heating caused by slight water absorption near 980 nm. This could be avoided by using a lower laser power density while extending the length of irradiation past 5 min.

C_{18}-PMH-mPEG was chosen as the exchanged biocompatible surfactant because of the favorable pharmacokinetics imparted on SWCNTs along with reduced immune response. Directly sonicated SWCNTs in C_{18}-PMH-mPEG display long circulation times[39] and high tumor accumulation;[13] the (6,5) SWCNTs exchanged into C18-PMH-mPEG displayed similar ultra-long circulation half-life and significant tumor uptake. Importantly, C_{18}-PMH-mPEG-coated SWCNTs

only partially activate the complement system, avoiding the generation of anaphylatoxins.[51] Specifically, the terminal pathway of the complement system is not triggered. This property has only been observed by C_{18}-PMH-mPEG surfactant coated SWCNTs; DSPE-mPEG, the surfactant previously used for exchanging SWCNTs,[4,21] was shown to fully activate the complement pathway.[51]

The poly(maleic anhydride) backbone forces the PEG to be spaced 1−1.5 nm apart, ideal for protein exclusion which prevents opsonization and removal from circulation. The ultra-long circulation time granted by the C_{18}-PMH-mPEG on SWCNTs enhances tumor accumulation more than targeting and allows the imaging/photothermal effect to be nonspecific for a range of cancers. To date, C_{18}-PMH-mPEG has been the most effective surfactant at delivering SWCNTs to tumor tissue, another important reason that it was chosen as the amphiphilic surfactant for exchange. The optimal, 1-D dimensions of the SWCNT construct creates the preferential accumulation in tumor tissue while the highly PEGylated exterior allows for sufficient circulation and stealth *in vivo* for the tumor accumulation to become significant compared to healthy tissue.

Homogenous solutions of a single diameter and narrow length distributions could help to address concerns over potential diameter-dependent cytotoxicity as well as the long-term fate of different diameters. Monodispersed solutions with a single nanotube species and well understood pharmacokinetics are much more likely to be used for future clinical use than an unsorted random mixture of diameters and electronic types. Furthermore, the selection of a SWCNT chirality with well-defined optical properties suited for a particular biological application can lead to dramatic decreases in the required dose while alleviating potential concerns over long-term retention toxicity. Further work is ongoing to investigate the long-term biodistribution/retention of SWCNTs and their chirality dependence, and excretion behaviors of the (6,5) SWCNTs as well as developing a well-defined toxicity profile of the highly homogeneous (6,5) SWCNTs.

CONCLUSION

There is an ongoing exploration for biocompatible *in vivo* imaging contrast agents for cancer diagnostics that possess high imaging sensitivity and resolution, provide excellent depth penetration, and that are deliverable. The ideal contrast agent should not only identify the site of a tumorous mass, but have intrinsic properties that provide noninvasive cancer therapy. As a bulk material, SWCNTs possess all the desired properties of a theranostic agent, with excellent tumor imaging and photothermal therapy at reasonable doses, yet lack structural homogeneity which profoundly influences their optical properties. Through this work, we have demonstrated the first system for making biocompatible, single-chirality SWCNTs through DGU and surfactant-exchange. The ultra-pure (6,5) SWCNTs replicated the pharmacokinetics, imaging, and photothermal capabilities of bulk SWCNTs at more than an order of magnitude lower dose. Tumors were unambiguously imaged and heated to 50 °C with an intravenous injection of ∼4 μg of SWCNT material. These results should spur future research into ultra-low dose, high efficiency SWCNT nanomedicines.

METHODS

Density Gradient Ultracentrifugation Separation of (6,5) SWCNT. Both iterations involve the creation of a density gradient by first pipetting six layers whose densities vary from 1.09 to 1.16 g/mL into a centrifuge tube followed by tilting the tube to 10° from horizontal for 1 h to allow for interlayer diffusion to smooth out the density steps. A constant surfactant loading of 0.7% sodium cholate and 0.175% sodium dodecyl sulfate throughout the centrifuge tube was used in the first iteration and the second iterative DGU step was performed with a 4:1 SC/SDS ratio and an overall surfactant loading of 1% (w/v). For the first iteration, SWCNTs, dispersed in 2% (w/v) SC + DI, were inserted in the gradient using a syringe pump. After 32 h of ultracentrifugation at 41 krpm, the purple (6,5) band was removed by lowering an HPLC needle fixed to a manual translational stage into the center of the band and removing 100 μL 3−4 times per centrifuge tube. The (6,5) extracted from the first iteration was placed at the bottom of a second linear density gradient using a syringe pump and run at 41 krpm for 14 h. Both centrifuge runs were performed on a SW41Ti rotor and an Optima L-100 XP Ultracentrifuge. See Supporting Information for all separation details.

Synthesis of 90 kDa C_{18}-PMH-mPEG. The 90 kDa amphiphilic poly(maleic anhydride-*alt*-1-octadecene)-methoxy poly(ethyleneglycol) (C_{18}-PMH-mPEG) was synthesized in the same manner as previously published.[39,52]

Surfactant Exchange from Sodium Cholate to 90 kDa C_{18}-PMH-mPEG. Ten milligrams of C_{18}-PMH-mPEG was added to 10 mL of (6,5) separated SWCNT solution at ∼0.01 mg SWCNT/mL concentration. The solution was bath sonicated for 5 min, and then placed in a 12−14 kDa molecular weight cutoff dialysis membrane and dialyzed in DI for 4 h. After 4 h, the solution was bath sonicated for 2 min and then placed back in the dialysis membrane with fresh water. This process was repeated through 8 water changes. The relative quantum yield of the solution was determined after each sonication by taking absorbance and NIR PL readings. After dialysis, the exchanged (6,5) SWCNT solution was washed 4× by centrifuge filtration with a 100 kDa MWCO filter (Millipore).

Near-Infrared Photoluminescence Imaging of Mice. Balb/c mice were purchased from Charles River and were housed at Stanford Research Animal Facility under Stanford Institutional Animal Care and Use Committee protocols.

For all mouse images, the mice were anesthetized on the imaging stage using 2 L/min O_2 flow mixed with 3% isoflurane. During imaging, an 808 nm laser diode (RMPC lasers) was focused on the imaging stage at 0.14 W/cm^2 irradiation power using an optical fiber and 4.5-mm focal length collimator (Thorlabs). The 808 nm excitation light source was filtered by an 850-nm short pass filter and a 1000-nm short pass filter (Thorlabs) to remove any stray light. NIR-II fluorescence emission was collected using a liquid-nitrogen-cooled, 320 × 256 pixel two-dimensional InGaAs array (Princeton Instruments) for collecting photons in NIR-II. The emission from the mice was filtered with a 900-nm long-pass filter (Thorlabs) before reaching the 2D InGaAs array detector to

remove autofluorescence. A lens pair consisting of two achromats (200 mm and 75 mm, Thorlabs) was used focus the image onto the detector with a field of view including the whole body of the mouse. All mouse images were taken with a 100 ms exposure time.

Photothermal Heating of (6,5) SWCNTs. For in solution heating, 100 μL of (6,5) SWCNTs having o.d.=1 at 991 nm (at a concentration of 3.2 μg/mL) was irradiated along with 50 μL of a control water solution and 50 μL of bulk HiPCO SWCNT solution. The solutions were irradiated with a 980 nm laser diode (VUEMetrix) with a 4.66 cm^2 spot size and 0.6 W/cm^2 irradiation power for 3 min. A MikroShot thermal camera (Mikron) was used to collect thermal images and quantify solution temperature every 30 s. For *in vivo* heating, the 15 4T1 tumor-bearing mice were anesthetized and irradiated with the 980 nm laser diode at 0.6 W/cm^2 and a 1.55 cm^2 spot size. During irradiation, thermal images were taken every minute as well as immediately before irradiation.

Blood Circulation and *ex Vivo* Biodistribution of SWCNTs. Three tumor bearing mice, with tumors located on each shoulder, were injected with (6,5) SWCNTs and used for circulation and biodistribution studies following previously established methods.[43] See Supporting Information for further details.

For experimental information on the characterization of SWCNT solutions, mouse handling, SWCNT injections, and photoluminescence excitation emission spectra of (6,5) and HiPCO SWCNTs, see Supporting Information.

Conflict of Interest: The authors declare no competing financial interest.

Supporting Information Available: Experimental methods, (6.5) separation details, (6,5) Raman characterization, surfactant exchange and length distributions, (6,5) mass balancing using the $\pi-\pi^*$ interband transition, toxicity and histology. This material is available free of charge *via* the Internet at http://pubs.acs.org.

Acknowledgment. This work was supported by the National Institutes of Health (NIH-NCI) (Grant 5R01A135109-02). This material is based upon work supported by the National Science Foundation Graduate Research Fellowship under Grant No. (DGE 1147470).

REFERENCES AND NOTES

1. Liu, Z.; Chen, K.; Davis, C.; Sherlock, S.; Cao, Q.; Chen, X.; Dai, H. J. Drug Delivery with Carbon Nanotubes for *in Vivo* Cancer Treatment. *Cancer Res.* **2008**, *68*, 6652–6660.
2. Robinson, J. T.; Welsher, K.; Tabakman, S. M.; Sherlock, S. P.; Wang, H.; Luong, R.; Dai, H. J. High Performance *in Vivo* Near-IR (>1 μm) Imaging and Photothermal Cancer Therapy with Carbon Nanotubes. *Nano Res.* **2010**, *3*, 779–793.
3. Liu, Z.; Cai, W.; He, L.; Nakayama, N.; Chen, K.; Sun, X.; Chen, X.; Dai, H. J. *In Vivo* Biodistribution and Highly Efficient Tumour Targeting of Carbon Nanotubes in Mice. *Nat. Nanotechnol.* **2007**, *2*, 47–52.
4. Welsher, K.; Liu, Z.; Sherlock, S. P.; Robinson, J. T.; Chen, Z.; Daranciang, D.; Dai, H. J. A Route to Brightly Fluorescent Carbon Nanotubes for Near-Infrared Imaging in Mice. *Nat. Nanotechnol.* **2009**, *4*, 773–780.
5. O'Connell, M. J.; Bachilo, S. M.; Huffman, C. B.; Moore, V. C.; Strano, M. S.; Haroz, E. H.; Rialon, K. L.; Boul, P. J.; Noon, W. H.; Kittrell, C.; et al. Band Gap Fluorescence from Individual Single-Walled Carbon Nanotubes. *Science* **2002**, *297*, 593–596.
6. Kam, N. W. S.; O'Connell, M.; Wisdom, J. A.; Dai, H. J. Carbon Nanotubes as Multifunctional Biological Transporters and Near-Infrared Agents for Selective Cancer Cell Destruction. *Proc. Natl. Acad. Sci. U.S.A.* **2005**, *102*, 11600–11605.
7. Bachilo, S. M.; Strano, M. S.; Kittrell, C.; Hauge, R. H.; Smalley, R. E.; Weisman, R. B. Structure-Assigned Optical Spectra of Single-Walled Carbon Nanotubes. *Science* **2002**, *298*, 2361–2366.
8. Welsher, K.; Sherlock, S. P.; Dai, H. J. Deep-Tissue Anatomical Imaging of Mice Using Carbon Nanotube Fluorophores in the Second Near-Infrared Window. *Proc. Natl. Acad. Sci. U.S.A.* **2011**, *108*, 8943–8948.
9. Heller, D. A.; Baik, S.; Eurell, T. E.; Strano, M. S. Single-Walled Carbon Nanotube Spectroscopy in Live Cells: Towards Long-Term Labels and Optical Sensors. *Adv. Mater.* **2005**, *17*, 2793–2799.
10. Hong, G. S.; Lee, J. C.; Robinson, J. T.; Raaz, U.; Xie, L.; Huang, N. F.; Cooke, J. P.; Dai, H. J. Multifunctional *in vivo* Vascular Imaging Using Near-Infrared II Fluorescence. *Nat. Med.* **2012**, *18*, 1841–1846.
11. Maeda, H.; Wu, J.; Sawa, T.; Matsumura, Y.; Hori, K. Tumor Vascular Permeability and the EPR Effect in Macromolecular Therapeutics: A Review. *J. Controlled Release* **2000**, *65*, 271–284.
12. Schipper, M. L.; Nakayama-Ratchford, N.; Davis, C. R.; Kam, N. W. S.; Chu, P.; Liu, Z.; Sun, X. M.; Dai, H. J.; Gambhir, S. S. A Pilot Toxicology Study of Single-Walled Carbon Nanotubes in a Small Sample of Mice. *Nat. Nanotechnol.* **2008**, *3*, 216–221.
13. Robinson, J. T.; Hong, G.; Liang, Y.; Zhang, B.; Yaghi, O. K.; Dai, H. J. *In Vivo* Fluorescence Imaging in the Second Near-Infrared Window with Long Circulating Carbon Nanotubes Capable of Ultrahigh Tumor Uptake. *J. Am. Chem. Soc.* **2012**, *134*, 10664–10669.
14. von Maltzahn, G.; Park, J. H.; Agrawal, A.; Bandaru, N. K.; Das, S. K.; Sailor, M. J.; Bhatia, S. N. Computationally Guided Photothermal Tumor Therapy Using Long-Circulating Gold Nanorod Antennas. *Cancer Res.* **2009**, *69*, 3892–3900.
15. Avouris, P.; Freitag, M.; Perebeinos, V. Carbon-Nanotube Photonics and Optoelectronics. *Nat. Photonics* **2008**, *2*, 341–350.
16. Green, A. A.; Hersam, M. C. Nearly Single-Chirality Single-Walled Carbon Nanotubes Produced via Orthogonal Iterative Density Gradient Ultracentrifugation. *Adv. Mater.* **2011**, *23*, 2185–2190.
17. Ha, M. J.; Xia, Y.; Green, A. A.; Zhang, W.; Renn, M. J.; Kim, C. H.; Hersam, M. C.; Frisbie, C. D. Printed, Sub-3V Digital Circuits on Plastic from Aqueous Carbon Nanotube Inks. *ACS Nano* **2010**, *4*, 4388–4395.
18. Chen, P. C.; Fu, Y.; Aminirad, R.; Wang, C.; Zhang, J. L.; Wang, K.; Galatsis, K.; Zhou, C. W. Fully Printed Separated Carbon Nanotube Thin Film Transistor Circuits and Its Application in Organic Light Emitting Diode Control. *Nano Lett.* **2011**, *11*, 5301–5308.
19. Tyler, T. P.; Brock, R. E.; Karmel, H. J.; Marks, T. J.; Hersam, M. C. Electronically Monodisperse Single-Walled Carbon Nanotube Thin Films as Transparent Conducting Anodes in Organic Photovoltaic Devices. *Adv. Energy Mater.* **2011**, *1*, 785–791.
20. Javey, A.; Guo, J.; Wang, Q.; Lundstrom, M.; Dai, H. J. Ballistic Carbon Nanotube Field-Effect Transistors. *Nature* **2003**, *424*, 654–657.
21. Diao, S.; Hong, G.; Robinson, J. T.; Jiao, L.; Antaris, A. L.; Wu, J. Z.; Choi, C. L.; Dai, H. J. Chirality Enriched (12,1) and (11,3) Single-Walled Carbon Nanotubes for Biological Imaging. *J. Am. Chem. Soc.* **2012**, *134*, 16971–16974.
22. Wu, J.; Xie, L.; Hong, G.; Lim, H. E.; Thendie, B.; Miyata, Y.; Shinohara, H.; Dai, H. D. Short Channel Field-Effect Transistors from Highly Enriched Semiconducting Carbon Nanotubes. *Nano Res.* **2012**, *5*, 388–394.
23. Tu, X. M.; Manohar, S.; Jagota, A.; Zheng, M. DNA Sequence Motifs for Structure-Specific Recognition and Separation of Carbon Nanotubes. *Nature* **2009**, *460*, 250–253.
24. Harutyunyan, A. R.; Chen, G. G.; Paronyan, T. M.; Pigos, E. M.; Kuznetsov, O. A.; Hewaparakrama, K.; Kim, S. M.; Zakharov, D.; Stach, E. A.; Sumanasekera, G. U. Preferential Growth of Single-Walled Carbon Nanotubes with Metallic Conductivity. *Science* **2009**, *326*, 116–120.
25. Kitiyanan, B.; Alvarez, W. E.; Harwell, J. H.; Resasco, D. E. Controlled Production of Single-Wall Carbon Nanotubes by Catalytic Decomposition of CO on Bimetallic Co-Mo Catalysts. *Chem. Phys. Lett.* **2000**, *317*, 497–503.
26. Zheng, M.; Semke, E. D. Enrichment of Single Chirality Carbon Nanotubes. *J. Am. Chem. Soc.* **2007**, *129*, 6084–6085.

27. Liu, H. P.; Nishide, D.; Tanaka, T.; Kataura, H. Large-Scale Single-Chirality Separation of Single-Wall Carbon Nanotubes by Simple Gel Chromatography. *Nat. Commun.* **2011**, *2*, 309.
28. Li, X. L.; Tu, X. M.; Zaric, S.; Welsher, K.; Seo, W. S.; Zhao, W.; Dai, H. J. Selective Synthesis Combined with Chemical Separation of Single-Walled Carbon Nanotubes for Chirality Selection. *J. Am. Chem. Soc.* **2007**, *129*, 15770–15771.
29. Hersam, M. C. Progress Towards Monodisperse Single-Walled Carbon Nanotubes. *Nat. Nanotechnol.* **2008**, *3*, 387–394.
30. Zhang, G. Y.; Qi, P. F.; Wang, X. R.; Lu, Y. R.; Li, X. L.; Tu, R.; Bangsaruntip, S.; Mann, D.; Zhang, L.; Dai, H. J. Selective Etching of Metallic Carbon Nanotubes by Gas-Phase Reaction. *Science* **2006**, *314*, 974–977.
31. Chattopadhyay, D.; Galeska, L.; Papadimitrakopoulos, F. A Route for Bulk Separation of Semiconducting from Metallic Single-Wall Carbon Nanotubes. *J. Am. Chem. Soc.* **2003**, *125*, 3370–3375.
32. Miyata, Y.; Shiozawa, K.; Asada, Y.; Ohno, Y.; Kitaura, R.; Mizutani, T.; Shinohara, H. Length-Sorted Semiconducting Carbon Nanotubes for High-Mobility Thin Film Transistors. *Nano Res.* **2011**, *4*, 963–970.
33. Moshammer, K.; Hennrich, F.; Kappes, M. M. Selective Suspension in Aqueous Sodium Dodecyl Sulfate According to Electronic Structure Type Allows Simple Separation of Metallic from Semiconducting Single-Walled Carbon Nanotubes. *Nano Res.* **2009**, *2*, 599–606.
34. Ghosh, S.; Bachilo, S. M.; Weisman, R. B. Advanced Sorting of Single-Walled Carbon Nanotubes by Nonlinear Density-Gradient Ultracentrifugation. *Nat. Nanotechnol.* **2010**, *5*, 443–450.
35. Dong, L.; Joseph, K. L.; Witkowski, C. M.; Craig, M. M. Cytotoxicity of Single-Walled Carbon Nanotubes Suspended in Various Surfactants. *Nanotechnology* **2008**, 19.
36. Zhang, L.; Tu, X. M.; Welsher, K.; Wang, X. R.; Zheng, M.; Dai, H. J. Optical Characterizations and Electronic Devices of Nearly Pure (10,5) Single-Walled Carbon Nanotubes. *J. Am. Chem. Soc.* **2009**, *131*, 2454–2455.
37. Arnold, M. S.; Green, A. A.; Hulvat, J. F.; Stupp, S. I.; Hersam, M. C. Sorting Carbon Nanotubes by Electronic Structure Using Density Differentiation. *Nat. Nanotechnol.* **2006**, *1*, 60–65.
38. Wenseleers, W.; Vlasov, I. I.; Goovaerts, E.; Obraztsova, E. D.; Lobach, A. S.; Bouwen, A. Efficient Isolation and Solubilization of Pristine Single-Walled Nanotubes in Bile Salt Micelles. *Adv. Funct. Mater.* **2004**, *14*, 1105–1112.
39. Prencipe, G.; Tabakman, S. M.; Welsher, K.; Liu, Z.; Goodwin, A. P.; Zhang, L.; Henry, J.; Dai, H. J. PEG Branched Polymer for Functionalization of Nanomaterials with Ultralong Blood Circulation. *J. Am. Chem. Soc.* **2009**, *131*, 4783–4787.
40. Murakami, Y.; Maruyama, S. Effect of Dielectric Environment on the Ultraviolet Optical Absorption of Single-Walled Carbon Nanotubes. *Phys. Rev. B* **2009**, 79.
41. Crochet, J. J.; Hoseinkhani, S.; Luer, L.; Hertel, T.; Doorn, S. K.; Lanzani, G. Free-Carrier Generation in Aggregates of Single-Wall Carbon Nanotubes by Photoexcitation in the Ultraviolet Regime. *Phys. Rev. Lett.* **2011**, 107.
42. Schoppler, F.; Mann, C.; Hain, T. C.; Neubauer, F. M.; Privitera, G.; Bonaccorso, F.; Chu, D. P.; Ferrari, A. C.; Hertel, T. Molar Extinction Coefficient of Single-Wall Carbon Nanotubes. *J. Phys. Chem. C* **2011**, *115*, 14682–14686.
43. Liu, Z.; Davis, C.; Cai, W. B.; He, L.; Chen, X. Y.; Dai, H. J. Circulation and Long-Term Fate of Functionalized, Biocompatible Single-Walled Carbon Nanotubes in Mice Probed by Raman spectroscopy. *Proc. Natl. Acad. Sci. U.S.A.* **2008**, *105*, 1410–1415.
44. Blackburn, J. L.; Holt, J. M.; Irurzun, V. M.; Resasco, D. E.; Rumbles, G. Confirmation of K-Momentum Dark Exciton Vibronic Sidebands Using ^{13}C-labeled, Highly Enriched (6,5) Single-walled Carbon Nanotubes. *Nano Lett.* **2012**, *12*, 1398–1403.
45. Lim, Y. T.; Kim, S.; Nakayama, A.; Stott, N. E.; Bawendi, M. G.; Frangioni, J. V. Selection of Quantum Dot Wavelengths for Biomedical Assays and Imaging. *Mol. Imaging* **2003**, *2*, 50–64.
46. Chen, J. Y.; Glaus, C.; Laforest, R.; Zhang, Q.; Yang, M. X.; Gidding, M.; Welch, M. J.; Xia, Y. N. Gold Nanocages as Photothermal Transducers for Cancer Treatment. *Small* **2010**, *6*, 811–817.
47. Yang, K.; Zhang, S. A.; Zhang, G. X.; Sun, X. M.; Lee, S. T.; Liu, Z. A. Graphene in Mice: Ultrahigh *in Vivo* Tumor Uptake and Efficient Photothermal Therapy. *Nano Lett.* **2010**, *10*, 3318–3323.
48. Liu, X.; Tao, H.; Yang, K.; Zhuang, S.; Lee, S.; Zhuang, L. Optimization of Surface Chemistry on Single-Walled Carbon Nanotubes for *in vivo* Photothermal Ablation of Tumors. *Biomaterials* **2011**, *32*, 144–151.
49. Ghosh, S.; Dutta, S.; Gomes, E.; Carroll, D.; D'Agostino, R.; Olson, J. J.; Guthold, M.; Gmeiner, W. H. Increased Heating Efficiency and Selective Thermal Ablation of Malignant Tissue with DNA-Encased Multiwalled Carbon Nanotubes. *ACS Nano* **2009**, *3*, 2667–2673.
50. Zhou, F.; Xing, D.; Ou, Z.; Wu, B.; Resasco, D. E.; Chen, W. R. Cancer Photothermal Therapy in the Near-Infrared Region by Using Single-Walled Carbon Nanotubes. *J. Biomed. Opt.* **2009**, 14.
51. Anderson, A. J.; Robinson, J. T.; Dai, H. J.; Hunter, A. C.; Andresen, T. L.; Moghimi, M. Single-Walled Carbon Nanotube Surface Control of Complement Recognition and Activation. *ACS Nano* **2013**, *7*, 1108–1119.
52. Robinson, J. T.; Tabakman, S. M.; Liang, Y.; Wang, H.; Casalongue, H. S.; Vinh, D.; Dai, H. J. Ultrasmall Reduced Graphene Oxide with High Near-Infrared Absorbance for Photothermal Therapy. *J. Am. Chem. Soc.* **2011**, *133*, 6825–6831.